Biophysical Journal, Volume *115*

Supplemental Information

Optimal Allocation of Bacterial Protein Resources under Nonlethal Protein Maturation Stress

Qing Zhang, Rui Li, Junbai Li, and Hualin Shi

Supporting Text

1 Experimental procedure and data processing methods

In order to derive the growth rate and β-galactosidase activity, we measured the absorbance of bacterial cells at 600nm (OD_{600}) and the absorbance of the product of β-galactosidase reaction at 405nm (OD_{405}) with a Wallac Victor3 1420 Multilabel Counter (PerkinElmer Life Sciences). The detailed experimental procedure, modified from the literature (1–3), are as follows. First, seed cultures were incubated in the M9 minimal growth medium with 0.2% (w/v) casamino acids and 0.5% (w/v) glucose (M9+cAA+Gluc) at 37°C (the same temperature was used for below cultivations). After ∼9 hours growth, the cultures were pelleted, washed at least once by centrifugation and resuspension with appropriate growth media and then inoculated in the media at initial $OD_{600} \approx 0.004$ for pre-cultures. After overnight growth, pre-cultures were pelleted, washed, and then inoculated in the experimental media with several concentrations of the growth inhibitor (chloramphenicol, paraquat or acetic acid), which were distributed to a 48-well plate (Corning Costar) in advance. The total volume of experimental culture per well was 1 mL. OD_{600} of the culture was measured no less than four times at an interval 30-50 minutes during the exponential phase (typically at OD_{600} between 0.03 and 0.18). During the late exponential phase (typically at OD_{600} between 0.12 and 0.18), removed 200μL culture per well to one 96-well plate (culture plate) and measured OD_{600} again. Added 160 μL permeabilization solution (0.8 mg/mL hexadecyltrimethylammonium bromide, 0.4 mg/mL sodium deoxycholate, 200 mM Na_2HPO_4, 20 mM KCl, 2 mM $MgSO_4$, and 5.4 μL/ml β-mercaptoethanol) per well to another 96-well plate (permeabilization plate), and removed 40 μL culture, which was in advance diluted fourfold with M9 salts solution (1L: 17.096g $Na_2HPO_4{\cdot}12H_2O$, 3g KH_2PO_4, 0.5g NaCl, 1g NH_4Cl, dissolved in ddH_2O), per well from the culture plate into the permeabilization solution. The permeabilization plate was kept at 4°C until all permeabilized samples were collected. To reduce the waiting time, the culture with more growth inhibitor was inoculated earlier with a larger initial OD_{600} (not exceeding 0.004). Next, added 190μL substrate solution (60mM Na_2HPO_4, 40 mM NaH_2PO_4, 10 mM KCl, 20 μg/mL hexadecyltrimethylammonium bromide, 10 μg/mL sodium deoxycholate, 1 mg/mL *o*-nitrophenyl-β-D-galactopyranoside, and 2.7 μL/mL β-mercaptoethanol) per well to another 96-well plate (reaction plate). Stored both the permeabilization and reaction plates at 30°C for ∼30 minutes. Then added 10μL permeabilized sample per well into the substrate solution and mixed them fully with a multichannel pipette. Immediately, the multilabel counter (PerkinElmer Life Sciences) was used to measure OD_{405} of the sample once per 1-3 minutes for 90 to 120 minutes at 30°C.

We obtained the growth rate by deriving the slope of the plot of the logarithm of OD_{600} during exponential phase versus the time. In earlier work (e.g (2, 3)), β-galactosidase activity was determined by deriving the slope of the plot of the product absorbance (at a wavelength of around 420nm) versus time. In our measurement, however, OD_{405} has a little concave-down tendency in the change with the time, which should result from that the product of the β-galactosidase reaction, i.e. o-nitrophenol (ONP), is steam volatile (4). We also observed that the color (yellow) of the product, unsealed and stored in the fume hood, turned much lighter after a few days, whereas that packaged hermetically lasted for several months. For simplicity, we assume that the detectable ONP decays slowly with a rate that is proportional to the concentration of ONP. We use x and y to denote concentrations of β-galactosidase and ONP, respectively. Then the change of y follows the differential equation

$$dy/dt = vx - \gamma y, \tag{1}$$

where v and γ denote the reaction rate per enzyme and decay constant, respectively. The solution can be derived as

$$y = vx(1 - e^{-\gamma t})/\gamma. \tag{2}$$

where vx and γ can be fixed by fitting the data of OD_{405} as a function of time with this equation (see examples in Figure S6 in the Supporting Material). Since vx represents the enzyme reaction rate per unit volume, β-galactosidase activity can be defined by

$$\beta - \text{gal activity(Miller units)} \triangleq 1000 \cdot vx \cdot \frac{1}{0.01} \times 20 \times \frac{1}{\mathrm{OD}_{600}} = 2 \times 10^6 \times \frac{vx}{\mathrm{OD}_{600}} \tag{3}$$

2 Analytically solving the optimization problem of protein allocation

2.1 Ignoring the toxicity of protein aggregates and without overexpression of the unnecessary protein

The optimization problem of protein allocation can be mapped into a two-dimensional space (ϕ_R, ϕ_{P2}). For simplicity, we define $\phi_{P0} = \phi_R - \phi_0$ and $\phi^{**} = \phi^* - \phi_0$. Then the constraints (Eqs. 15-18 in the main text) become

$$\begin{aligned}
(b\phi_{P0} + \phi_{P2} - \phi^{**})(k_1 - k_3) &\geq 0, &(4)\\
(a\phi_{P0} + \phi_{P2} - \phi^{**})(k_3 - k_1) &\geq 0, &(5)\\
\phi_{P0}\phi_m/(\phi_m + \phi_{P2}) - (a-b)^{-1}(a\phi_{P0} + \phi_{P2} - \phi^{**}) &\geq 0, &(6)\\
\phi_{P0}, \phi_{P2} &\geq 0, &(7)
\end{aligned}$$

where $a = 1 + k_0/k_1$ and $b = 1 + k_0/k_3$. The objective is to maximize

$$\mu = k_0\phi_{P0}\phi_{P2}/(\phi_m + \phi_{P2}). \tag{8}$$

This two-dimensional nonlinear programming problem can be solved analytically and strictly. Obviously, the optimum (maximum) is not at $\phi_{P0} = 0$ or $\phi_{P2} = 0$. When $\phi_{P0}, \phi_{P1} > 0$, we have $\partial\mu/\partial\phi_{P0} > 0$ and $\partial\mu/\partial\phi_{P2} > 0$. So the optimum should be located at the boundary of the region defined by Eqs. 4-7. With the boundary condition, the optimum can be derived directly. Thus we obtain the optimal allocation solution ϕ_{P0}^{opt} (ϕ_R^{opt}), ϕ_{P2}^{opt} and the maximized growth rate μ_{max}. Then ϕ_{P1}^{opt} and ϕ_{P3}^{opt} can be derived from Eqs. 15 and 17 in the main text. Furthermore, we can formalize the relationship of the optimal allocation fractions and growth rate under the stress that reduces flux capacity k_1,k_0 or $1/\phi_m$.

As below, we give the analytic solution in two cases, from which we represent the proteome fraction of each class proteins as a function of growth rate. (i) If $k_1 > k_3$, we have $J_3 = 0$ and $J_0 = J_1$. Then the optimal allocation is

$$\begin{aligned}
\phi_R^{opt} &= \frac{k_1}{k_0 + k_1}(\phi_m + \phi^{**})^{1/2}\left[(\phi_m + \phi^{**})^{1/2} - \phi_m^{1/2}\right] + \phi_0, &(9)\\
\phi_{P1}^{opt} &= \frac{k_0}{k_0 + k_1}(\phi_m + \phi^{**})^{1/2}\left[(\phi_m + \phi^{**})^{1/2} - \phi_m^{1/2}\right], &(10)\\
\phi_{P2}^{opt} &= \phi_m^{1/2}\left[(\phi_m + \phi^{**})^{1/2} - \phi_m^{1/2}\right], &(11)\\
\phi_{P3}^{opt} &= 0, &(12)
\end{aligned}$$

and the maximized growth rate is

$$\mu_{max} = \frac{k_0 k_1}{k_0 + k_1}\left[(\phi_m + \phi^{**})^{1/2} - \phi_m^{1/2}\right]^2. \tag{13}$$

Next, we present the correlation of allocation fractions and bacterial growth rate under three limitations. (1) Under AA supply limitation (k_1 declining), ϕ_{P2}^{opt} and ϕ_{P3}^{opt} are constant, while ϕ_R^{opt} and ϕ_{P1}^{opt} can be expressed as linear functions of growth rate by

$$\begin{aligned}
\phi_R^{opt} &= A\mu_{max}/(k_0 B) + \phi_0, &(14)\\
\phi_{P1}^{opt} &= -A\mu_{max}/(k_0 B) + AB, &(15)
\end{aligned}$$

where $A = (\phi_m + \phi^{**})^{1/2}$ and $B = (\phi_m + \phi^{**})^{1/2} - \phi_m^{1/2}$. As can be seen from Eqs. 14-15, ϕ_R^{opt} positively correlates with growth rate, whereas ϕ_{P1}^{opt} negatively correlates with growth rate. (2) Under translation limitation (k_0 decreasing), ϕ_{P2}^{opt} and ϕ_{P3}^{opt} are still constant, while ϕ_R^{opt} and ϕ_{P1}^{opt} can be expressed as linear functions of growth rate by

$$\begin{aligned}
\phi_R^{opt} &= -A\mu_{max}/(k_1 B) + AB + \phi_0, &(16)\\
\phi_{P1}^{opt} &= A\mu_{max}/(k_1 B). &(17)
\end{aligned}$$

From Eqs. 16-17, ϕ_R^{opt} negatively depends on growth rate, whereas ϕ_{P1}^{opt} positively depends on growth rate. (3) Under UP maturation limitation (ϕ_m increasing), ϕ_{P3}^{opt} are still constant, and ϕ_R^{opt}, ϕ_{P1}^{opt} and ϕ_{P2}^{opt} can be expressed as linear functions of growth rate by

$$\begin{aligned}
\phi_R^{opt} &= 0.5\mu_{max}/k_1 + 0.5\phi^{**}k_0/(k_0+k1) + \phi_0, && (18)\\
\phi_{P1}^{opt} &= 0.5\mu_{max}/k_0 + 0.5\phi^{**}k_1/(k_0+k1), && (19)\\
\phi_{P2}^{opt} &= -0.5(1/k_0 + 1/k_1)\mu_{max} + 0.5\phi^{**}. && (20)
\end{aligned}$$

From Eqs. 18-20, as the growth rate increases, ϕ_R^{opt} and ϕ_{P1}^{opt} increase, whereas ϕ_{P2}^{opt} decreases.

(ii) If $k_1 < k_3$, we have $J_5 = 0$, $J_4 = J_3$ and $J_2 = J_1$. Then the optimal allocation is

$$\begin{aligned}
\phi_R^{opt} &= \frac{k_1}{k_0+k_1}\left[(c\phi_m+\phi^{**})^{1/2} - (c\phi_m)^{1/2}\right]\left[(c\phi_m+\phi^{**})^{1/2} - (c\phi_m)^{1/2} + (\phi_m/c)^{1/2}\right] + \phi_0, && (21)\\
\phi_{P1}^{opt} &= \frac{k_0}{k_0+k_1}\left[(c\phi_m+\phi^{**})^{1/2} - (c\phi_m)^{1/2}\right]^2, && (22)\\
\phi_{P2}^{opt} &= (c\phi_m)^{1/2}\left[(c\phi_m+\phi^{**})^{1/2} - (c\phi_m)^{1/2}\right], && (23)\\
\phi_{P3}^{opt} &= \frac{k_0}{k_0+k_3}(c\phi_m)^{1/2}\left[(c\phi_m+\phi^{**})^{1/2} - (c\phi_m)^{1/2}\right], && (24)
\end{aligned}$$

and the maximized growth rate is

$$\mu_{max} = \frac{k_0k_1}{k_0+k_1}\left[(c\phi_m+\phi^{**})^{1/2} - (c\phi_m)^{1/2}\right]^2, \quad (25)$$

where $c(=b/a) = (1+k_0/k_3)\,/\,(1+k_0/k_1)$. In the following we study the dependence of the allocation fractions on growth rate under three limitations. (1) Under AA supply limitation (k_1 declining), ϕ_R^{opt}, ϕ_{P1}^{opt}, ϕ_{P2}^{opt} and ϕ_{P3}^{opt} can be expressed as functions of growth rate by

$$\begin{aligned}
\phi_R^{opt} &= \mu_{max}/k_0 + \left[k_3\phi_m/(k_0(k_0+k_3))\right]^{1/2}\mu_{max}^{1/2} + \phi_0, && (26)\\
\phi_{P1}^{opt} &= -\mu_{max}/k_0 - 2[(k_0+k_3)\phi_m/(k_0k_3)]^{1/2}\mu_{max}^{1/2} + \phi^{**}, && (27)\\
\phi_{P2}^{opt} &= \left[(k_0+k_3)\phi_m/(k_0k_3)\right]^{1/2}\mu_{max}^{1/2}, && (28)\\
\phi_{P3}^{opt} &= \left[k_0\phi_m/((k_0+k_3)k_3)\right]^{1/2}\mu_{max}^{1/2}. && (29)
\end{aligned}$$

From Eqs. 26-29, ϕ_R^{opt} and ϕ_{P1}^{opt} are quadratic functions of $\mu_{max}^{1/2}$, while ϕ_{P2}^{opt} and ϕ_{P3}^{opt} are linear functions of $\mu_{max}^{1/2}$. (2) Under translation limitation (k_0 decreasing), ϕ_R^{opt}, ϕ_{P1}^{opt}, ϕ_{P2}^{opt} and ϕ_{P3}^{opt} can be expressed as functions of growth rate by

$$\begin{aligned}
\phi_R^{opt} &= (f(\mu_{max})^2 - \mu_{max}/k_3)(1+\phi_m^{1/2}/f(\mu_{max})) + \phi_0, && (30)\\
\phi_{P1}^{opt} &= \mu_{max}/k_1, && (31)\\
\phi_{P2}^{opt} &= \phi_m^{1/2}f(\mu_{max}), && (32)\\
\phi_{P3}^{opt} &= \phi_m^{1/2}\mu_{max}/(k_3f(\mu_{max})). && (33)
\end{aligned}$$

where $f(\mu_{max}) = [(1/k_3 - 1/k_1)\mu_{max} + \phi_m + \phi^{**}]^{1/2} - \phi_m^{1/2}$. From Eqs. 30-33, ϕ_R^{opt} and ϕ_{P2}^{opt} negatively correlate with growth rate, ϕ_{P1}^{opt} linearly and positively correlates with growth rate, while ϕ_{P3}^{opt} positively correlates with growth rate. (3) Under UP maturation limitation (ϕ_m increasing), ϕ_R^{opt}, ϕ_{P1}^{opt}, ϕ_{P2}^{opt} and ϕ_{P3}^{opt} can be expressed as linear functions of growth rate by

$$\begin{aligned}
\phi_R^{opt} &= \mu_{max}/k_0 - k_3(k_0+k_1)\mu_{max}/[2k_0k_1(k_0+k_3)] + 0.5k_3\phi^{**}/(k_0+k_3) + \phi_0, && (34)\\
\phi_{P1}^{opt} &= \mu_{max}/k_1, && (35)\\
\phi_{P2}^{opt} &= -(k_0+k_1)\mu_{max}/(2k_0k_1) + 0.5\phi^{**}, && (36)\\
\phi_{P3}^{opt} &= -(k_0+k_1)\mu_{max}/[2(k_0+k_3)k_1] + 0.5k_0\phi^{**}/(k_0+k_3). && (37)
\end{aligned}$$

We know from Eqs. 34-37, as the growth rate increases, ϕ_{P1}^{opt} linearly increases, ϕ_{P2}^{opt} and ϕ_{P3}^{opt} linearly decrease, while ϕ_R^{opt} linearly increases when $k_1 > k_0k_3/(2k_0+k_3)$ but linearly decreases when $k_1 < k_0k_3/(2k_0+k_3)$.

2.2 Considering the toxicity of protein aggregates

By considering the toxicity of protein aggregate in the model, we can investigate how protein aggregates affect protein allocation. Protein aggregates probably interfere with many cellular processes, but the main mechanism resulting in their toxicity is still unclear. One plausible mechanism works by protein aggregates interfering with the maturation of proteins. Thus we can add the interference of protein aggregates with the maturation of proteins in the model. We redefine the aberrant maturation flux J_4 in Eq. 7 in the main text as

$$J_4 = k_4\psi_{UP}K_m/(K_m + \psi_{P2}) + k_6\psi_{PA}\psi_{UP}, \tag{38}$$

where the new term $k_6\psi_{PA}\psi_{UP}$ indicates the interference effect, and k_6 is constant. Then Eq. 12 in the main text becomes

$$\mu = J_2 = k_0(\phi_R - \phi_0)\phi_{P2}/\left[(1 + \gamma_1\phi_{PA})\phi_{P2} + (1 + \gamma_2\phi_{PA})\phi_m\right] \tag{39}$$

where $\gamma_1 \triangleq k_6\psi_{NP}/k_2$ and $\gamma_2 \triangleq k_6\psi_{NP}/k_4$.

We can analytically solve this optimization problem by mapping it into a two-dimensional space(ϕ_{P0}, ϕ_{P2}). For the sake of convenience, we take $k_2 = k_4$, so $\gamma_1 = \gamma_2 \triangleq \gamma$. If $\gamma \geq \phi^{**}/(\phi^{**} + \phi_m)$, the constraints and objective function are the same as shown by formulas 4-8, and the results are shown by Eqs. 21-25. If $\gamma < \phi^{**}/(\phi^{**} + \phi_m)$, the constraints can be described by formulas 4, 5, 7 and

$$\phi_{P0}\phi_m/(\phi_m + \phi_{P2}) \leq (a - b)^{-1}[a\phi_{P0} + \phi_{P2} - \phi^{**}]; \tag{40}$$

and the objective function can be expressed as

$$\mu = (1 - \gamma)^{-1}k_0\left[\phi_{P0}\phi_{P2}/(\phi_m + \phi_{P2}) - \gamma(b - a)^{-1}(b\phi_{P0} + \phi_{P2} - \phi^{**})\right] \tag{41}$$

where $a = 1+k_0/k_1$ and $b = 1+k_0/k_3$. Define $A = (\phi_m+\phi^{**})^{1/2}-\phi_m^{1/2}(1-\gamma)^{-1/2}$ and $B = \left(\phi^{**}/A - A\right)^2/4\phi_m$ (>1). When $c(= b/a) < B$, the results are the same as shown by Eqs. 21-25. When $c > B$, the optimal allocation is

$$\begin{aligned}
\phi_R^{opt} &= \frac{k_1}{k_1 + k_0}(\phi_m + \phi^{**})^{1/2}\left[(\phi_m + \phi^{**})^{1/2} - \phi_m^{1/2}(1 - \gamma)^{-1/2}\right] + \phi_0, &(42)\\
\phi_{P1}^{opt} &= \frac{k_0}{k_0 + k_1}(\phi_m + \phi^{**})^{1/2}\left[(\phi_m + \phi^{**})^{1/2} - \phi_m^{1/2}(1 - \gamma)^{-1/2}\right], &(43)\\
\phi_{P2}^{opt} &= \phi_m^{1/2}\left[(\phi_m + \phi^{**})^{1/2}(1 - \gamma)^{-1/2} - \phi_m^{1/2}\right], &(44)\\
\phi_{P3}^{opt} &= 0, &(45)
\end{aligned}$$

and the maximized growth rate is

$$\mu_{max} = \frac{k_0k_1}{k_0 + k_1}\left[(\phi_m + \phi^{**})^{1/2} - \phi_m^{1/2}(1 - \gamma)^{-1/2}\right]^2. \tag{46}$$

The above analytical solutions show that if the toxicity of protein aggregates is large enough ($\gamma \geqslant (\phi^* - \phi_0)/(\phi^* - \phi_0 + \phi_m)$), bacteria will degrade all the aberrant proteins without the jump taking place in the relation of protein allocation and growth rate. Otherwise ($\gamma < (\phi^* - \phi_0)/(\phi^* - \phi_0 + \phi_m)$), the bacteria will either degrade all aberrant proteins or allow all of them to aggregate, and which way to choose is determined by physiological conditions. Moreover, the jump point will change, and when AA supply capacity is larger than the jump point, the toxicity will make mass fractions of ribosome-affiliated proteins and AA supply-required proteins (ϕ_R^{opt} and ϕ_{P1}^{opt}) and the growth rate μ_{max} decrease while the mass fraction of chaperones (ϕ_{P2}^{opt}) increase.

2.3 Overexpression of unnecessary protein

Overexpression of the unnecessary protein directly affects three fluxes: translation flux (J_0), maturation flux (J_2) and the aberrant maturation flux J_4. In order to consider the effects in our model, we partition these three fluxes into two groups of sub-fluxes: one group for the unnecessary protein (J_0^U, J_2^U and J_4^U) while another for the needed proteins (J_0^N, J_2^N and J_4^N). This is helpful to address the optimization problem of protein allocation when the maturation

frustration levels of the unnecessary protein (ϕ_m^U) and the useful proteins (ϕ_m^N) are not the same. Referring to Eqs. 10, 12 and 14 in the main text, these sub-fluxes can be represented by

$$\begin{aligned} J_0^N &= k_0\phi_{P0}^N, && (47)\\ J_2^N &= k_0\phi_{P0}^N\phi_{P2}/(\phi_m^N+\phi_{P2}), && (48)\\ J_4^N &= k_0\phi_{P0}^N\phi_m^N/(\phi_m^N+\phi_{P2}), && (49) \end{aligned}$$

and

$$\begin{aligned} J_0^U &= k_0\phi_{P0}^U, && (50)\\ J_2^U &= k_0\phi_{P0}^U\phi_{P2}/(\phi_m^U+\phi_{P2}), && (51)\\ J_4^U &= k_0\phi_{P0}^U\phi_m^U/(\phi_m^U+\phi_{P2}), && (52) \end{aligned}$$

where the variables labeled with N are for native proteins, while those labeled with U are for unnecessary proteins. ϕ_{P0}^N and ϕ_{P0}^U indicate mass fractions of active R-sector proteins (ribosome-affiliated proteins) for needed proteins and unnecessary protein, respectively and $\phi_{P0}^N+\phi_{P0}^U=\phi_R-\phi_0$. Accordingly, the constraints on the fluxes become

$$\begin{aligned} J_1+J_3 &= J_0^N+J_0^U && (53)\\ J_0^N &= J_2^N+J_4^N && (54)\\ J_0^U &= J_2^U+J_4^U && (55)\\ J_4^N+J_4^U &= J_3+J_5 && (56)\\ J_2^N &= \mu(1-\phi_U) && (57)\\ J_2^U &= \mu\phi_U && (58) \end{aligned}$$

The normalization condition is

$$\phi_{P0}^N+\phi_{P0}^U+\phi_{P1}+\phi_{P2}+\phi_{P3}=\phi_R^{\max}-\phi_0-\phi_U\triangleq\phi^{***} \quad (59)$$

Based on the upregulation of many chaperones in response to overexpression of unnecessary protein (5, 6), we assign the mass fraction of all chaperones (ϕ_{P2}) to an unoptimizable part (proportional to ϕ_U) and an optimizable part ($\tilde{\phi}_{P2}$), represented by (see the main text)

$$\phi_{P2}=\tilde{\phi}_{P2}+\alpha\phi_U \quad (60)$$

where $\tilde{\phi}_{P2}\geq 0$ and α is constant. Notice that here $\phi_{P2}\geq\alpha\phi_U$, i.e. chaperones has a minimal mass fraction $\alpha\phi_U$. When $\alpha=0$ and $\phi_m\approx 0$, our model is equivalent to that of Scott et al. (3).

Based on Eqs. 47-60 and the condition $k_1>k_3$, we can solve the optimization problem in a one-dimensional space. First, we can obtain $\phi_{P3}^{opt}=0$ and derive

$$\mu=\phi_{P2}(\phi^{***}-\phi_{P2})/[\tilde{k}(\phi_{P2}+\tilde{\phi}_m)] \quad (61)$$

where $\tilde{k}=(k_0+k_1)/(k_0k_1)$ and $\tilde{\phi}_m=(1-\phi_U)\phi_m^N+\phi_U\phi_m^U$. If $\alpha\phi_U\leq\sqrt{(\tilde{\phi}_m+\phi^{***})\tilde{\phi}_m}-\tilde{\phi}_m$, the maximal growth rate and the optimal mass fraction of P_2-class proteins are

$$\begin{aligned} \mu_{max} &= \left(\sqrt{\tilde{\phi}_m+\phi^{***}}-\sqrt{\tilde{\phi}_m}\right)^2/\tilde{k}. && (62)\\ \phi_{P2}^{opt} &= \sqrt{(\tilde{\phi}_m+\phi^{***})\tilde{\phi}_m}-\tilde{\phi}_m. && (63) \end{aligned}$$

If $\alpha\phi_U>\sqrt{(\tilde{\phi}_m+\phi^{***})\tilde{\phi}_m}-\tilde{\phi}_m$, we have

$$\begin{aligned} \mu_{\max} &= \alpha\phi_U(\phi^{***}-\alpha\phi_U)/[\tilde{k}(\alpha\phi_U+\tilde{\phi}_m)], && (64)\\ \phi_{P2}^{opt} &= \alpha\phi_U. && (65) \end{aligned}$$

Then with the formulas

$$\begin{aligned}
\phi_{P0}^{N} &= \mu_{\max}(1-\phi_U)(1+\phi_m^N/\phi_{P2}^{opt})/k_0, && (66)\\
\phi_{P0}^{U} &= \mu_{\max}\phi_U(1+\phi_m^U/\phi_{P2}^{opt})/k_0, && (67)\\
\phi_R &= \phi_{P0}^N+\phi_{P0}^U+\phi_0, && (68)\\
\phi_{P1} &= k_0\phi_R/k_1, && (69)
\end{aligned}$$

we can derive $\phi_{P0}^{N,opt}$, $\phi_{P0}^{U,opt}$, ϕ_R and ϕ_{P1}^{opt}, respectively.

Finally, we list the optimal solution and the maximal growth rate as below: (i) If $\alpha\phi_U \le \sqrt{(\tilde{\phi}_m+\phi^{***})\tilde{\phi}_m}-\tilde{\phi}_m$, the maximized growth rate and the optimal allocation fractions are

$$\begin{aligned}
\mu_{max} &= k_0k_1\left(\sqrt{\tilde{\phi}_m+\phi^{***}}-\sqrt{\tilde{\phi}_m}\right)^2/(k_0+k_1), && (70)\\
\phi_{P0}^{N,opt} &= \frac{k_1(1-\phi_U)}{k_0+k_1}\left(\sqrt{1+\phi^{***}/\tilde{\phi}_m}-1\right)\left(\sqrt{(\tilde{\phi}_m+\phi^{***})\tilde{\phi}_m}+\phi_U(\phi_m^N-\phi_m^U)\right), && (71)\\
\phi_{P0}^{U,opt} &= \frac{k_1\phi_U}{k_0+k_1}\left(\sqrt{1+\phi^{***}/\tilde{\phi}_m}-1\right)\left(\sqrt{(\tilde{\phi}_m+\phi^{***})\tilde{\phi}_m}+(1-\phi_U)(\phi_m^U-\phi_m^N)\right), && (72)\\
\phi_R^{opt} &= \frac{k_1}{k_0+k_1}\left(\sqrt{1+\phi^{***}/\tilde{\phi}_m}-1\right)\sqrt{(\tilde{\phi}_m+\phi^{***})\tilde{\phi}_m}+\phi_0, && (73)\\
\phi_{P1}^{opt} &= \frac{k_0}{k_0+k_1}\left(\sqrt{1+\phi^{***}/\tilde{\phi}_m}-1\right)\sqrt{(\tilde{\phi}_m+\phi^{***})\tilde{\phi}_m}, && (74)\\
\phi_{P2}^{opt} &= \sqrt{(\tilde{\phi}_m+\phi^{***})\tilde{\phi}_m}-\tilde{\phi}_m, && (75)\\
\phi_{P3}^{opt} &= 0 && (76)
\end{aligned}$$

where $\tilde{\phi}_m = (1-\phi_U)\phi_m^N+\phi_U\phi_m^U$. (ii) If $\alpha\phi_U > \sqrt{(\tilde{\phi}_m+\phi^{***})\tilde{\phi}_m}-\tilde{\phi}_m$, the maximized growth rate and the optimal allocation fractions are

$$\begin{aligned}
\mu_{\max} &= \alpha\phi_Uk_0k_1(\phi^{***}-\alpha\phi_U)/[(k_0+k_1)(\alpha\phi_U+\tilde{\phi}_m)], && (77)\\
\phi_{P0}^{N,opt} &= \frac{k_1}{k_0+k_1}(1-\phi_U)(\phi^{***}-\alpha\phi_U)(\alpha\phi_U+\phi_m^N)/(\alpha\phi_U+\tilde{\phi}_m), && (78)\\
\phi_{P0}^{U,opt} &= \frac{k_1}{k_0+k_1}\phi_U(\phi^{***}-\alpha\phi_U)(\alpha\phi_U+\phi_m^U)/(\alpha\phi_U+\tilde{\phi}_m), && (79)\\
\phi_R^{opt} &= \frac{k_1}{k_0+k_1}(\phi^{***}-\alpha\phi_U)+\phi_0, && (80)\\
\phi_{P1}^{opt} &= \frac{k_0}{k_0+k_1}(\phi^{***}-\alpha\phi_U), && (81)\\
\phi_{P2}^{opt} &= \alpha\phi_U, && (82)\\
\phi_{P3}^{opt} &= 0. && (83)
\end{aligned}$$

Here we obtain the optimal solution even when the maturation frustration levels ϕ_m^U and ϕ_m^N are different from each other. We assigned different values to ϕ_m^U (its difference from ϕ_m^N is not too large), but the results did not change much. So we consider the simplest case $\phi_m^U = \phi_m^N \triangleq \phi_m$ in fitting the experimental data.

When $\phi_m^U = \phi_m^N$, actually, we do not need to separate the translation flux and the normally and aberrantly maturation fluxes as above (one for the useless protein and another for needed proteins). In this case, the model can still be described by Eqs. 10-18 in the main text, but the normalization condition (i.e. Eq. 17 in the main text) should be changed to

$$\phi_R+\phi_{P1}+\phi_{P2}+\phi_{P3} = \phi_R^{\max}-\phi_U \triangleq \phi^{***} \quad (84)$$

where $\phi_U \geqslant 0$. We still assign the mass fraction of all chaperones (ϕ_{P2}) to an unoptimizable part (proportional to ϕ_U) and an optimizable part ($\tilde{\phi}_{P2}$) as above, represented by Eq. 60. Then the analytic results under the condition $k_1 > k_3$

are: (i) If $\alpha\phi_U \leq \sqrt{(\phi_m+\phi^{***})\phi_m}-\phi_m$, the maximized growth rate and the optimal allocation fractions are

$$\mu_{max} = k_0k_1\left(\sqrt{\phi_m+\phi^{***}}-\sqrt{\phi_m}\right)^2/(k_0+k_1), \quad (85)$$

$$\phi_R^{opt} = \frac{k_1}{k_0+k_1}\left(\sqrt{1+\phi^{***}/\phi_m}-1\right)\sqrt{(\phi_m+\phi^{***})\phi_m}+\phi_0, \quad (86)$$

$$\phi_{P1}^{opt} = \frac{k_0}{k_0+k_1}\left(\sqrt{1+\phi^{***}/\phi_m}-1\right)\sqrt{(\phi_m+\phi^{***})\phi_m}, \quad (87)$$

$$\phi_{P2}^{opt} = \sqrt{(\phi_m+\phi^{***})\phi_m}-\phi_m, \quad (88)$$

$$\phi_{P3}^{opt} = 0. \quad (89)$$

(ii) If $\alpha\phi_U > \sqrt{(\phi_m+\phi^{***})\phi_m}-\phi_m$, the maximized growth rate and the optimal allocation fractions are

$$\mu_{\max} = \alpha\phi_U k_0k_1(\phi^{***}-\alpha\phi_U)/[(k_0+k_1)(\alpha\phi_U+\phi_m)], \quad (90)$$

$$\phi_R^{opt} = \frac{k_1}{k_0+k_1}(\phi^{***}-\alpha\phi_U)+\phi_0, \quad (91)$$

$$\phi_{P1}^{opt} = \frac{k_0}{k_0+k_1}(\phi^{***}-\alpha\phi_U), \quad (92)$$

$$\phi_{P2}^{opt} = \alpha\phi_U, \quad (93)$$

$$\phi_{P3}^{opt} = 0. \quad (94)$$

Clearly, when $\phi_m^U=\phi_m^N\triangleq\phi_m$, $\tilde{\phi}_m=\phi_m$, so Eqs. 70-83 decay to Eqs. 85-94.

3 The model predicts optimal allocation of proteins under the limitation on flux capacity (when $k_1 < k_3$)

In the main text, we mainly show the change of protein allocation with growth rate under the limitation on one flux capacity when AA supply capacity (k_1) is larger than AP degradation capacity (k_3), i.e. $k_1 > k_3$. Here we additionally give the results under the condition $k_1 < k_3$ (see Figure S3 and S4 in the Supporting Material). Figure S3 *A*, obtained by rescaling X-axis of Figure 3 *A*, more clearly shows that there is a jump in protein allocation at a growth rate of ∼0.15 doublings/hour. When $k_1 < k_3$, the exponential steady-state may occur in some special cases. For example, when the bacteria are grown in the MOPS minimal medium with 0.2% glycerol+20 mM Threonine (7). Figure S3 *B* presents the results under translation limitation when $k_1(=0.09h^{-1}) < k_3(=0.3h^{-1})$, some of which are significantly different from those under the condition $k_1 > k_3$: the mass fraction of chaperones and other affiliated proteins (ϕ_{P2}) increases (from 2.8% to 4.9%) while the mass fraction of proteases (ϕ_{P3}) decreases (from 2.7% to 0) with the growth rate decreasing (from 0.055 dbls/h to 0 dbls/h). These are likely testable predictions.

Under the protein maturation stress (e.g. thermal, acidic or oxidative stress), the mass fraction of chaperones and other protein factors promoting maturation (ϕ_{P2}) increase with the stress intensity (ϕ_m) (see Table 1 and Figures 3 *C* and Figures S3 *C*). When AA supply capacity is smaller than AP degradation capacity ($k_1 < k_3$), ϕ_R^{opt} is nearly constant and close to ϕ_0, both ϕ_{P2}^{opt} and ϕ_{P3}^{opt} linearly increase, whereas ϕ_{P1}^{opt} linearly decreases with the growth rate decreasing (Figure S3 *C*). In addition, Figure S4 shows that the aberrant maturation flux (J_4) totally shifts to the degradation flux (J_3) when $k_1 < k_3$, which is in line with the above results.

4 The theoretical explanation for experimental data under translation, acidic and oxidative stresses

The model gives the ratios of protein allocation, while what we measured is β-galactosidase activity (Z), reflecting the concentration of β-galactosidase (ψ_Z). We will derive a formula to link ψ_Z with the allocation ratios. First, we have

$$Z \propto \psi_Z = \phi_Z\psi_{NP}. \quad (95)$$

Then we will represent ψ_{NP} by a function of ϕ_R. The bacterial cell mass (M_c) consists of protein mass (M_{NP}), RNA mass (M_{rna}), DNA mass (M_{dna}) and the mass of other constituents (M_{other}), namely,

$$M_c = M_{NP} + M_{rna} + M_{dna} + M_{other}. \tag{96}$$

Dividing both sides by M_c, we obtain

$$1 = \psi_{NP} + \psi_{rna} + \psi_{dna} + \psi_{other}. \tag{97}$$

Because

$$\psi_{rna} = \phi_R \psi_{NP}/\rho, \tag{98}$$

where $\rho = M_R/M_{rna} = 0.76$ (3), we derive

$$\psi_{NP} = \rho(1 - \psi_{dna} - \psi_{other})/(\rho + \phi_R). \tag{99}$$

The experimental data of Basan et al. (8) shows that ψ_{other} is independent of the growth rate μ and $\psi_{dna} \ll 1$, so we approximately have

$$\psi_{NP} \propto 1/(\rho + \phi_R). \tag{100}$$

Equation 100 provides good fits to experimental data of Bremer and Dennis (9) and Basan et al. (8) as shown in Figure S7 in the Supporting Material. As proposed by Scott et al. (3), the mass fraction of β-galactosidase driven by a constitutive promoter should be proportional to that of P_1-class proteins, i.e.

$$\phi_Z \propto \phi_{P1}. \tag{101}$$

Substituting Eqs. 100 and 101 into equation 95, we have

$$Z = C\phi_{P1}/(\rho + \phi_R), \tag{102}$$

where C is a scaling factor independent of growth rate.

In fitting experimental data, we take the flux capacities that are limited by the stress as variables and assign proper values to the parameters including the unaffected flux capacities (see Table S1 in the Supporting Material). Under the chloramphenicol stress, translational flux is limited, and then we view k_0 as a variable. Under the oxidative/acidic stress, we consider that both AA supply and protein maturation fluxes are limited. Thus we take k_1 and ϕ_m as variables and denote their values in the absence of oxidative/acidic stress as k_1^* and ϕ_m^*, respectively. We use $x = \phi_m/\phi_m^* - 1$ to indicate the stress intensity, leading to $\phi_m = \phi_m^*(1+x)$. Furthermore, we assume $k_1 = k_1^*/[1+(x/K_x)^\beta]$, where K_x (equilibrium constant) and β (Hill coefficient) can be inferred by fitting experimental data. Parameters k_0 and k_1 (or k_1^*) are chosen properly based on those used by Scott et al. (3). The stress intensity x is a function of the concentration of the inducer (acetic acid or paraquat) and $x = 0$ indicates the case without the stress.

5 Molecular mechanisms adjusting protein allocation in *E.coli*

The sigma factor, as a subunit of RNA polymerase, recognizes the promoter to initiate the transcription. Different sigma factors have different biases to the sequence of the promoter. In *E.coli*, in addition to the housekeeping sigma factor (σ^D), six alternative sigma factors (σ^S, σ^N, σ^H, σ^E, σ^F and σ^{FecI}) have been identified (10, 11). Stress stimuli lead to up-regulation of some alternative sigma factors and concomitantly up-regulation of the proteins regulated by these alternative factors whereas the housekeeping sigma factor and its regulated proteins are down-regulated in level and activity(12, 13). Different sigma factors compete to bind the core RNAP (E) and the regulation of their competition is an effective strategy to adjust protein allocation (12, 13). Many global factors, such as ppGpp, Rsd, Crl, CRP, Fis, IHF, HNS, and 6S RNA, regulate the number and the activity of sigma factors and some of them are growth rate-dependent, such as ppGpp, Rsd and 6S RNA (14, 15). In this scenario, ppGpp, as an effector of the stringent response, represses the transcription of rRNA directly and thereby inhibits the synthesis of ribosome-affiliated proteins (3, 16, 17). In the bacterial adaptation to the stress, it is possible that multiple growth rate-dependent global regulators cooperatively regulate the competition between different σ factors for core RNAPs and the competition between different mRNAs for ribosomes to achieve the reallocation of the proteome (12).

The bacterial transcript levels parallel protein levels in average (18, 19). Therefore, protein level can be roughly determined by *mRNA* level (m) and translation initiation rate (l), i.e.

$$\phi_R : \phi_{P1} : \phi_{P2} : \phi_{P3} = l_0 m_0 : l_1 m_1 : l_2 m_2 : l_3 m_3. \tag{103}$$

The concentration of each class *mRNA* (m_i) has an approximate linear relationship with concentrations of free RNAP holoenzyme ($[E\sigma^j]_f$)

$$m_i = \frac{1}{\beta_i} \sum_{j \in J} \alpha_i^j N_i^j [E\sigma^j]_f, \tag{104}$$

where the class set of σ factors $J \triangleq \{D,\ S,\ N,\ H,\ E,\ F,\ FecI\}$ for *E.coli*, α_i^j and N_i^j denote average transcriptional strength and the number of P_i-class promoters recognized by σ^j, respectively and β_i indicates the degradation rate of the ith-class mRNA. We assume that $[E\sigma^j]_f$ and the total concentration of σ^j are correlated as

$$[E\sigma^j]_f = \lambda_j [\sigma^j], \tag{105}$$

where λ_j is related to free E concentration, affinity of σ_j with E, availability of specific/nonspecific RNAP binding sites on DNA and corresponding strength of RNAP binding to them (13). Define

$$r_j = [\sigma^j] / (\sum_{j' \in J} [\sigma^{j'}]), \tag{106}$$

where the total concentration of sigma factors $\sum_{j \in J} [\sigma^j]$ is basically independent of the growth rate (20). Then, we have

$$\phi_R : \phi_{P1} : \phi_{P2} : \phi_{P3} = \sum_{j \in J} A_0^j r_j : \sum_{j \in J} A_1^j r_j : \sum_{j \in J} A_2^j r_j : \sum_{j \in J} A_3^j r_j \tag{107}$$

where $A_i^j = l_i \alpha_i^j N_i^j \lambda_j / \beta_i$. There are two normalization conditions:

$$\phi_R + \sum_{i=1}^{3} \phi_{Pi} = \phi^*, \tag{108}$$

$$\sum_{j \in J} r_j = 1. \tag{109}$$

Then protein reallocation in some specific stress adaptation can be understood from the change of r_j and A_i^j.

In *E.coli* stress adaptation, the regulation of the competition between sigma factors can affect the ratio r_j (12, 21). In another way, ppGpp inhibits the synthesis of rRNA and some ribosomal proteins, and moreover, ribosomal proteins that are not assembled into ribosomes repress their own translational initiation (l_0 and A_0^j decreasing) by the mechanism of "translation feedback of ribosomal proteins" (17). Based on the knowledge on specific promoters recognized by each sigma factor in *E.coli* (10, 11), we consider $A_0^{\{S,\ N,\ E,\ F,\ FecI\}} = 0$, $A_2^{\{N,\ FecI\}} = 0$ and $A_3^{\{N,\ FecI\}} = 0$. Then, we can estimate the variation tendency of protein allocation in three cases. (i) When carbon source is limited, $r_{\{N,\ H,\ E,\ F,\ FecI\}} \approx 0$ and $\phi_{P2} + \phi_{P3} \approx 0$. From Eqs. 107-109, we approximately have

$$\phi_R : \phi_{P1} \approx (A_0^D r_D) : (A_1^D r_D + A_1^S r_S), \tag{110}$$

$$\Delta(\phi_R + \phi_{P1}) \approx 0, \tag{111}$$

$$\Delta(r_D + r_S) \approx 0. \tag{112}$$

Limitation of carbon source induces the emergence of stringent factor ppGpp and some other regulators, which lead to $\Delta l_0 < 0$, $\Delta r_D < 0$ and $\Delta r_S > 0$ (12, 17, 21). Then we derive $\Delta\phi_R < 0$ and $\Delta\phi_{P1} > 0$. (ii) Under the stress induced by chloramphenicol, translational process will be inhibited (3). Then the concentration of spoT ppGpp synthetase and the concentration of ppGpp will be reduced (3, 22). Thus $l_0(A_0^j)$ and r_D will be larger, whereas r_S will be smaller (12, 17, 21). Further considering $\Delta r_{\{N,\ H,\ E,\ F,\ FecI\}} \approx 0$ and Eqs. 110-112, we have that ϕ_R rises and ϕ_{P1} declines. (iii) In acidic/oxidative/thermal stress adaptation, empirical data imply that $\Delta r_{\{H,\ E,\ S\}} > 0$, $\Delta r_D < 0$ and

$\Delta A_0^D < 0$ (23–33). Moreover, we consider $\Delta r_{\{N,\ F,\ FecI\}} = 0$, $A_0^H r_H \ll A_0^D r_D$, $A_1^S r_S + A_1^H r_H + A_1^E r_E \ll A_1^D r_D$, $A_2^D r_D \ll A_2^H r_H + A_2^E r_E + A_2^S r_S$ and $A_3^D r_D \ll A_3^H r_H + A_3^E r_E + A_3^S r_S$. Then according to Eqs. 107-109, we have

$$\phi_R : \phi_{P1} : \phi_{P2} : \phi_{P3} \approx (A_0^D r_D) : (A_1^D r_D) : (A_2^H r_H + A_2^E r_E + A_2^S r_S) : (A_3^H r_H + A_3^E r_E + A_3^S r_S) \qquad (113)$$

Based on this equation and the above assumption, ϕ_{P2} and ϕ_{P3} will increase, ϕ_R will decrease, whereas ϕ_{P1} will either increase or decrease.

References

1. Zhang, X., and H. Bremer, 1995. Control of the Escherichia coli rrnB P1 promoter strength by ppGpp. *J. Biol. Chem.* 270:11181–11189.

2. Shetty, R. P., 2008. Applying engineering principles to the design and construction of transcriptional devices. Ph.D. thesis, Massachusetts Institute of Technology. Biological Engineering Division. `http://hdl.handle.net/1721.1/41843`.

3. Scott, M., C. W. Gunderson, E. M. Mateescu, Z. Zhang, and T. Hwa, 2010. Interdependence of cell growth and gene expression: origins and consequences. *Science* 330:1099–1102.

4. Sidgwick, N. V., and W. M. Aldous, 1921. CVIII.-Influence of position on the solubility and volatility of the mono-and di-nitrophenols. *J. Chem. Soc., Trans.* 119:1001–1012.

5. Dong, H., L. Nilsson, and C. G. Kurland, 1995. Gratuitous overexpression of genes in Escherichia coli leads to growth inhibition and ribosome destruction. *J. Bacteriol.* 177:1497–1504.

6. Oh, M.-K., and J. C. Liao, 2000. DNA microarray detection of metabolic responses to protein overproduction in Escherichia coli. *Metab. Eng.* 2:201–209.

7. Dai, X., M. Zhu, M. Warren, R. Balakrishnan, V. Patsalo, H. Okano, J. R. Williamson, K. Fredrick, Y.-P. Wang, and T. Hwa, 2016. Reduction of translating ribosomes enables Escherichia coli to maintain elongation rates during slow growth. *Nat. Microbiol.* 2:16231.

8. Basan, M., M. Zhu, X. Dai, M. Warren, D. Sévin, Y.-P. Wang, and T. Hwa, 2015. Inflating bacterial cells by increased protein synthesis. *Mol. Syst. Biol.* 11:836.

9. Bremer, H., and P. P. Dennis, 1996. Modulation of chemical composition and other parameters of the cell by growth rate. *In* F. C. Neidhardt, R. Curtiss III, J. L. Ingraham, E. C. C. LIN, K. B. Low, B. Magasanik, W. S. Reznikoff, M. Riley, M. Schaechter, and H. E. Umbarger, editors, Escherichia coli and Salmonella: Cellular and Molecular Biology, 2nd ed., American Society for Microbiology, Washington, DC, USA, volume 2, pp. 1553–1569.

10. Gama-Castro, S., H. Salgado, A. Santos-Zavaleta, D. Ledezma-Tejeida, L. Muñiz-Rascado, J. S. García-Sotelo, K. Alquicira-Hernández, I. Martínez-Flores, L. Pannier, J. A. Castro-Mondragón, et al., 2015. RegulonDB version 9.0: high-level integration of gene regulation, coexpression, motif clustering and beyond. *Nucleic Acids Res.* 44:D133–D143.

11. Keseler, I. M., A. Mackie, A. Santos-Zavaleta, R. Billington, C. Bonavides-Martínez, R. Caspi, C. Fulcher, S. Gama-Castro, A. Kothari, M. Krummenacker, et al., 2017. The EcoCyc database: reflecting new knowledge about Escherichia coli K-12. *Nucleic Acids Res.* 45:D543–D550.

12. Nyström, T., 2004. MicroReview: Growth versus maintenance: a trade-off dictated by RNA polymerase availability and sigma factor competition? *Mol. Microbiol.* 54:855–862.

13. Grigorova, I. L., N. J. Phleger, V. K. Mutalik, and C. A. Gross, 2006. Insights into transcriptional regulation and σ competition from an equilibrium model of RNA polymerase binding to DNA. *Proc. Natl. Acad. Sci. U.S.A.* 103:5332–5337.

14. Campbell, E. A., L. F. Westblade, and S. A. Darst, 2008. Regulation of bacterial RNA polymerase σ factor activity: a structural perspective. *Curr. Opin. Microbiol.* 11:121–127.

15. Sharma, U. K., and D. Chatterji, 2010. Transcriptional switching in Escherichia coli during stress and starvation by modulation of σ70 activity. *FEMS Microbiol. Rev.* 34:646–657.

16. Paul, B. J., W. Ross, T. Gaal, and R. L. Gourse, 2004. rRNA transcription in Escherichia coli. *Annu. Rev. Genet.* 38:749–770.

17. Kaczanowska, M., and M. Rydén-Aulin, 2007. Ribosome biogenesis and the translation process in Escherichia coli. *Microbiol. Mol. Biol. Rev.* 71:477–494.

18. Conway, T., and G. K. Schoolnik, 2003. Microarray expression profiling: capturing a genome-wide portrait of the transcriptome. *Mol. Microbiol.* 47:879–889.

19. Taniguchi, Y., P. J. Choi, G.-W. Li, H. Chen, M. Babu, J. Hearn, A. Emili, and X. S. Xie, 2010. Quantifying E. coli proteome and transcriptome with single-molecule sensitivity in single cells. *Science* 329:533–538.

20. Iwakura, Y., K. Ito, and A. Ishihama, 1974. Biosynthesis of RNA polymerase in Escherichia coli.I. Control of RNA polymerase content at various growth rates. *Mol. Gen. Genet.* 133:1–23.

21. Jishage, M., K. Kvint, V. Shingler, and T. Nyström, 2002. Regulation of ς factor competition by the alarmone ppGpp. *Genes Dev.* 16:1260–1270.

22. Bremer, H., and P. Dennis, 2008. Feedback control of ribosome function in Escherichia coli. *Biochimie* 90:493–499.

23. Farr, S. B., and T. Kogoma, 1991. Oxidative stress responses in Escherichia coli and Salmonella typhimurium. *Microbiol. Rev.* 55:561–585.

24. Guisbert, E., T. Yura, V. A. Rhodius, and C. A. Gross, 2008. Convergence of molecular, modeling, and systems approaches for an understanding of the Escherichia coli heat shock response. *Microbiol. Mol. Biol. Rev.* 72:545–554.

25. Malki, A., H.-T. Le, S. Milles, R. Kern, T. Caldas, J. Abdallah, and G. Richarme, 2008. Solubilization of protein aggregates by the acid stress chaperones HdeA and HdeB. *J. Biol. Chem.* 283:13679–13687.

26. Hong, W., Y. E. Wu, X. Fu, and Z. Chang, 2012. Chaperone-dependent mechanisms for acid resistance in enteric bacteria. *Trends Microbiol.* 20:328–335.

27. Dahl, J.-U., M. J. Gray, and U. Jakob, 2015. Protein quality control under oxidative stress conditions. *J. Mol. Biol.* 427:1549–1563.

28. Tucker, D. L., N. Tucker, and T. Conway, 2002. Gene expression profiling of the pH response in Escherichia coli. *J. Bacteriol.* 184:6551.

29. Maurer, L. M., E. Yohannes, S. S. Bondurant, M. Radmacher, and J. L. Slonczewski, 2005. pH regulates genes for flagellar motility, catabolism, and oxidative stress in Escherichia coli K-12. *J. Bacteriol.* 187:304–319.

30. Allen, K. J., and M. W. Griffiths, 2012. Impact of hydroxyl-and superoxide anion-based oxidative stress on logarithmic and stationary phase Escherichia coli O157: H7 stress and virulence gene expression. *Food Microbiol.* 29:141–147.

31. Foshag, D., E. Henrich, E. Hiller, M. Schäfer, C. Kerger, A. Burger-Kentischer, I. Diaz-Moreno, S. M. García-Mauriño, V. Dötsch, S. Rupp, et al., 2017. The E. coli S30 lysate proteome: A prototype for cell-free protein production. *New Biotechnol.* .

32. Chen, K., Y. Gao, N. Mih, E. J. O'Brien, L. Yang, and B. O. Palsson, 2017. Thermosensitivity of growth is determined by chaperone-mediated proteome reallocation. *Proc. Natl. Acad. Sci. U.S.A.* 114:11548.

33. Schmidt, A., K. Kochanowski, S. Vedelaar, E. Ahrné, B. Volkmer, L. Callipo, K. Knoops, M. Bauer, R. Aebersold, and M. Heinemann, 2016. The quantitative and condition-dependent Escherichia coli proteome. *Nat. Biotechnol.* 34:104–110.

34. Liebermeister, W., E. Noor, A. Flamholz, D. Davidi, J. Bernhardt, and R. Milo, 2014. Visual account of protein investment in cellular functions. *Proc. Natl. Acad. Sci. U.S.A.* 111:8488–8493.

35. Valgepea, K., K. Adamberg, A. Seiman, and R. Vilu, 2013. Escherichia coli achieves faster growth by increasing catalytic and translation rates of proteins. *Mol. BioSyst.* 9:2344–2358.

36. Li, G.-W., D. Burkhardt, C. Gross, and J. S. Weissman, 2014. Quantifying absolute protein synthesis rates reveals principles underlying allocation of cellular resources. *Cell* 157:624–635.

37. Hui, S., J. M. Silverman, S. S. Chen, D. W. Erickson, M. Basan, J. Wang, T. Hwa, and J. R. Williamson, 2015. Quantitative proteomic analysis reveals a simple strategy of global resource allocation in bacteria. *Mol. Syst. Biol.* 11:784.

Supporting Figures

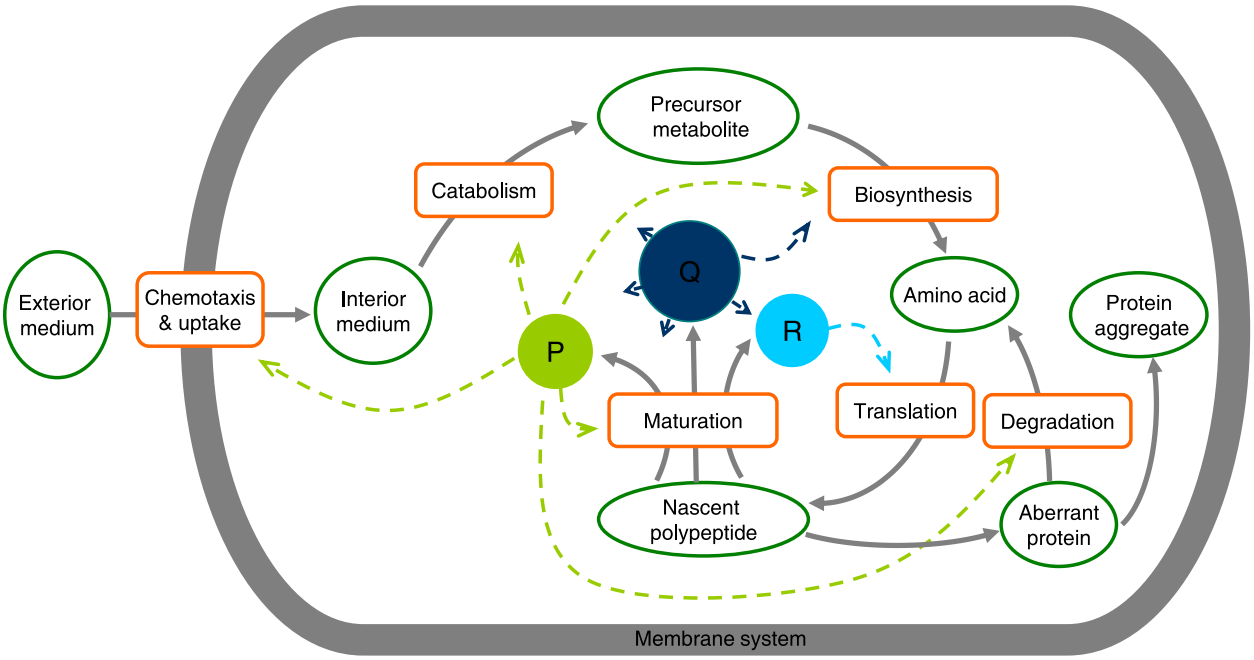

Figure S1: An schematic diagram for the main processes of protein self-production. Squares denote main biochemical reaction pathways during protein producing. Circles indicate substrates, intermediate products or final products. The normally matured proteins are partitioned into three classes: Q (housekeeping and growth rate-independent proteins), R (ribosome-affiliated proteins) and P (others). The allocations of P, Q and R classes of proteins are indicated by dashed lines. R-class proteins are devoted to the translation process. P-class proteins are devoted to the processes of amino acid supply (chemotaxis, nutrient uptake, catabolism and biosynthesis), nascent polypeptides maturation and aberrant proteins degradation. Q-class proteins are devoted to the biosynthesis process and many other processes.

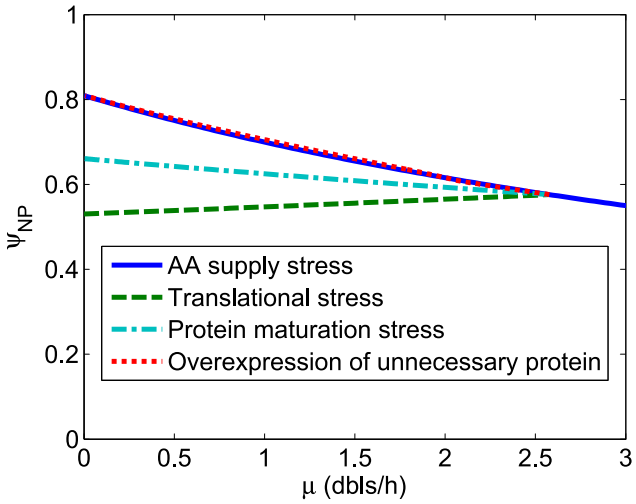

Figure S2: The concentration of normal proteins, i.e. the fraction of cell mass occupied by normal protein mass (ψ_{NP}), slightly depends on the growth rate under the stresses considered in this study. The cell mass here does not include the mass of protein aggregates. Protein aggregates as wastes from protein production contribute little to the normal physiological processes inside the cell, and they usually occupy the isolated space (e.g. in the form of inclusion body). Therefore, it is reasonable to refer to the concentration in the remaining connected space. Moreover, Eq .99, i.e. $\psi_{NP} = (1 - \psi_{dna} - \psi_{other})/(1 + \phi_R/\rho)$, was used, where $\rho = 0.76$ (3) and $\psi_{dna} + \psi_{other} = 0.12$ (8).

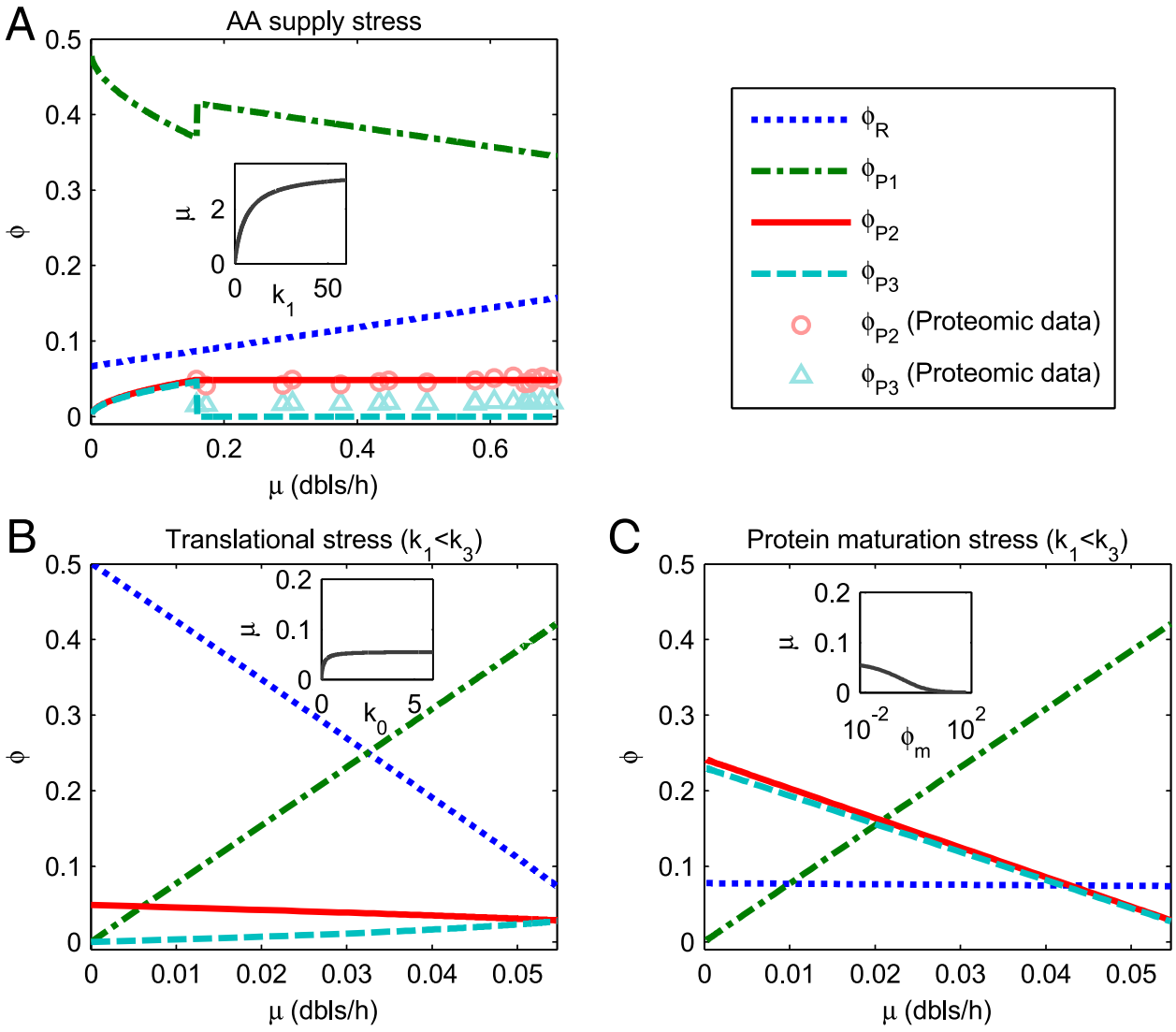

Figure S3: **The model predicts the relation of protein allocation fractions and the growth rate when one flux capacity (k_1, k_0 or $1/\phi_m$) is reduced by the stress.** The plots mainly show the results when $k_1 < k_3$. Insets present the decrease of growth rate with flux capacity limitation, in which units of μ, k_1, k_0, and ϕ_m are doublings/hour $(dbls/h)$, h^{-1}, h^{-1}, and 1 respectively. ϕ_R, ϕ_{P1}, ϕ_{P2}, and ϕ_{P3} indicate proteome fractions of ribosome-affiliated proteins (R-class), AA supply-required proteins (P_1-class), chaperone-like proteins (P_2-class), and protease-like proteins (P_3-class), respectively. The experimental data for ϕ_{P2} (circles) and ϕ_{P3} (triangles) are obtained with the classification of Proteomaps (34) and those in (A) are based on the proteomic data of ref. (33, 35–37), and those in (B) based on ref. (37). Common parameters: $\phi^* = 0.55$, $\phi_0 = 0.066$, $k_3 = 0.3h^{-1}$. (A) AA supply stress shown by k_1 decreasing. Parameters: $k_0 = 6h^{-1}$ and $\phi_m = 0.0061$. (B)Translational stress displayed by k_0 decreasing ($k_1 < k_3$). Parameters: $k_1 = 0.09h^{-1}$ and $\phi_m = 0.0061$ (C) Protein maturation stress reflected by ϕ_m increasing ($k_1 < k_3$). Parameters: $k_0 = 6h^{-1}$ and $k_1 = 0.09h^{-1}$.

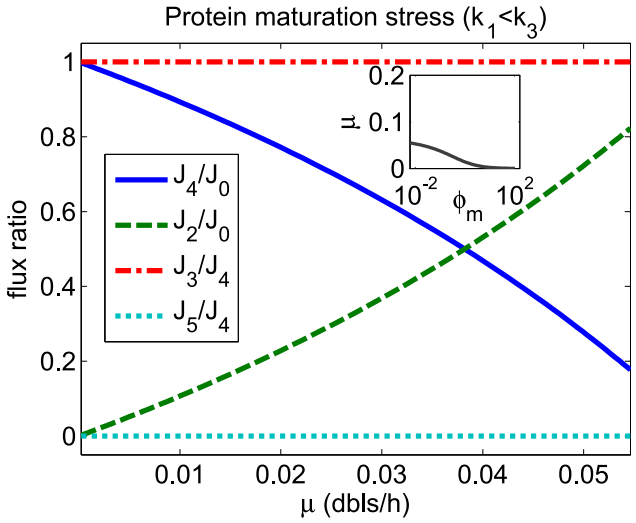

Figure S4: **Translation flux shifts from the normal maturation flux to the aberrant maturation flux under protein maturation stress (ϕ_m increasing).** J_0: translation flux; J_2: normal maturation flux; J_4: aberrant maturation flux; J_3: degradation flux; J_5: aggregation flux. J_2/J_0 and J_4/J_0 indicate fractions of nascent polypeptides matured normally and abnormally, respectively. J_3/J_4 and J_5/J_4 indicate fractions of aberrant proteins degraded and aggregating, respectively. Notice that $J_2/J_0 + J_4/J_0 = 1$ and $J_3/J_4 + J_5/J_4 = 1$. The plot shows that J_2/J_0 decreases with the maturation stress (minimum=0), whereas J_4/J_0 increases with the maturation stress (maximum=1). When AA supply capacity is smaller than the degradation capacity ($k_1 < k_3$), AP degradation flux is switched on and all the aberrantly matured proteins are degraded. Parameters are the same as that used in Fig. S3.

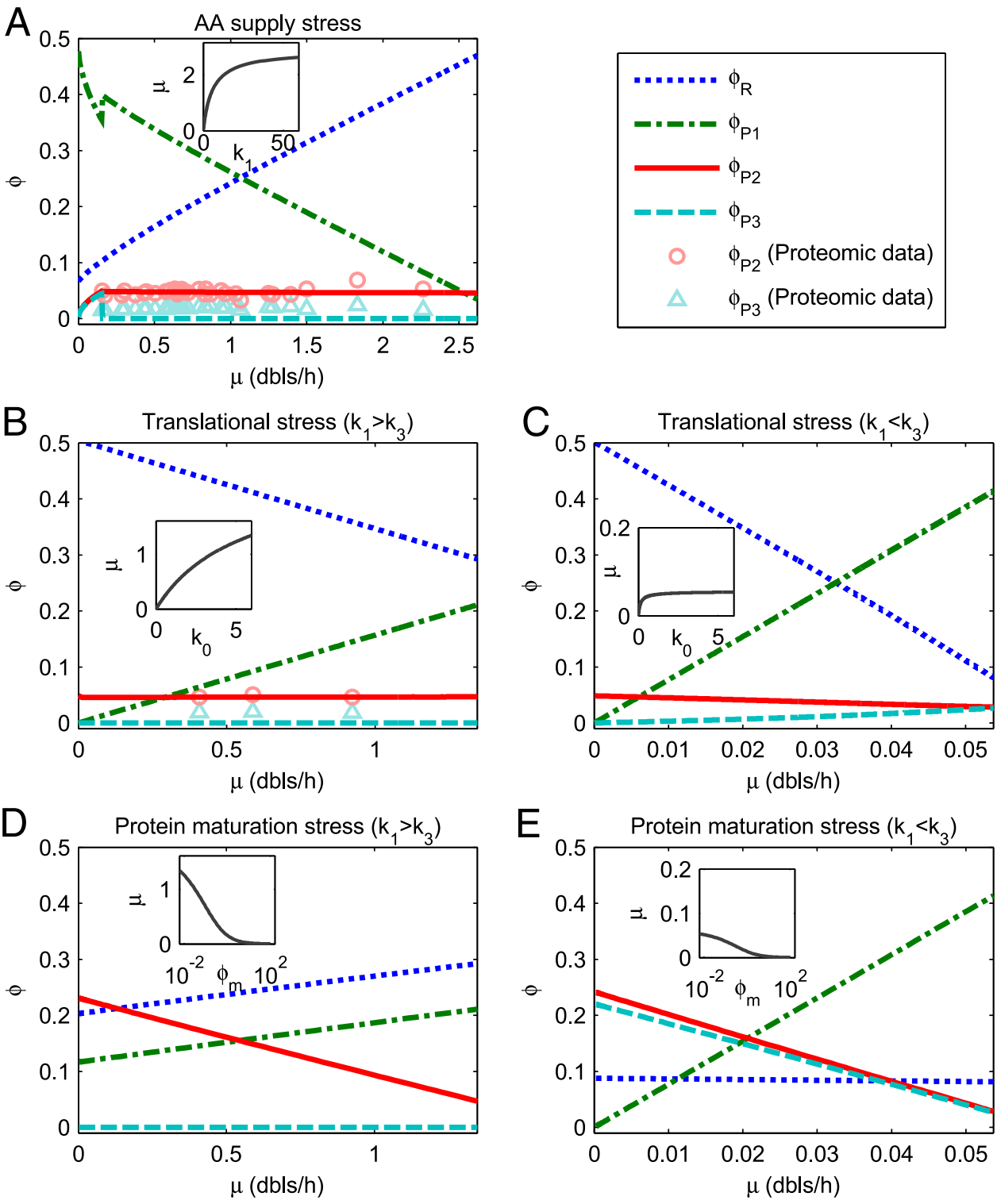

Figure S5: **Consideration of growth rate-dependence of translational capacity k_0 does not affect the theoretical relationship of protein allocation fractions and growth rate much when one flux capacity (k_1, k_0 or $1/\phi_m$) is reduced by the stress.** Insets present the decrease of growth rate with flux capacity limitation, in which units of μ, k_1, k_0, and ϕ_m are $dbls/h$, h^{-1}, h^{-1}, and 1 respectively. ϕ_R, ϕ_{P1}, ϕ_{P2} and ϕ_{P3} indicate proteome fractions of ribosome-affiliated proteins (R-class), AA supply-required proteins (P_1-class), chaperone-like proteins (P_2-class) and protease-like proteins (P_3-class), respectively. Experimental data for ϕ_{P2} (circles) and ϕ_{P3} (triangles) are obtained with the classification of Proteomaps (34) and those in (A) are based on the proteomic data of ref. (33, 35–37), and those in (B) based on ref. (37). Parameters are the same as those in Fig. 3 and Fig.S3: (A)-Fig. 3 *A*, (B)-Fig. 3 *B*, (C)-Fig. S3 *B*, (D)-Fig. 3 *C*, (E)-Fig. S3 *C*.

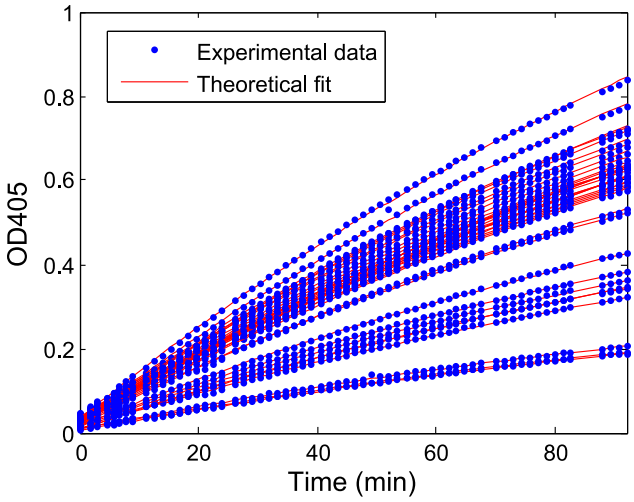

Figure S6: Examples for fitting the data of OD405 as a function of time from β-galactosidase assay. Blue dots denote experimental data. Red lines indicate the theoretical fits with Eq. 2. Decay constant $\gamma = 0.006$ (for every line).

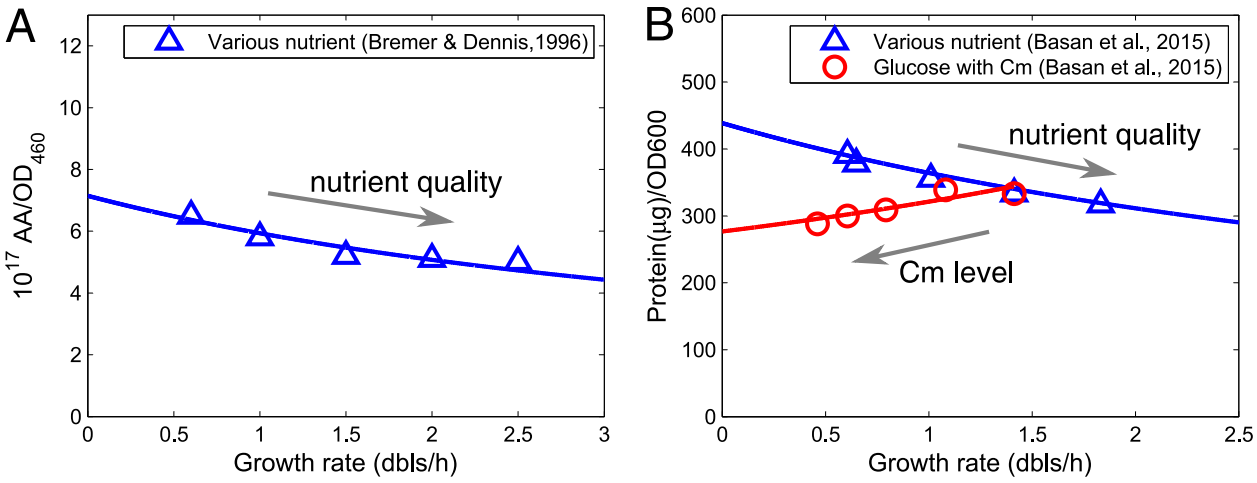

Figure S7: Equation 100 well fits the experimental relationship between the ratio of total protein mass to cell mass and growth rate. Blue triangles denote experimental data with various nutrient. Red circles denote experimental data with different chloramphenicol (Cm) levels. Lines indicate corresponding fits with Eq. 100. For simplicity, the linear relations $\phi_R = \phi_0 + \mu/5.92$ (for various nutrient) and $\phi_R = \phi_R^{\max} - \mu/5.5$ (for glucose with Cm) were used (based on (3)). (A) Fitting experimental data of Bremer and Dennis (9). The fitted scaling factor is 5.53 $\times 10^{17}\mathrm{AA/OD}_{460}$. (B) Fitting experimental data of Basan et al. (8). The fitted scaling factor is 362 $\mu g/\mathrm{OD}_{600}$.

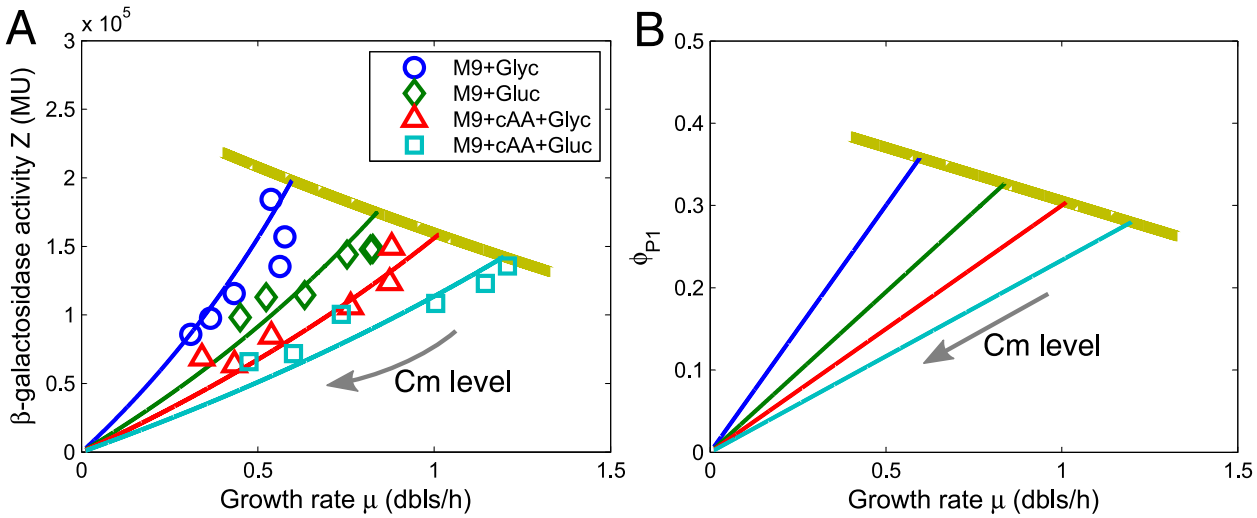

Figure S8: Relationship between β-galactosidase activity (A) or proteome fraction of P_1-class protein (B) and growth rate under translational inhibition induced by chloramphenicol (Cm). Circles, diamonds, triangles, and squares denote experimental results for bacteria cultivated in four different growth media (M9+Glyc, M9+Gluc, M9+cAA+Glyc and M9+cAA+Gluc) with different sublethal levels of chloramphenicol. Corresponding experimental data are shown in Table S4. Blue, green, red, and cyan lines indicate theoretical results under translational stress, whereas the yellow lines under AA supply stress. Theoretical parameters are $\phi^* = 0.55$, $\phi_0 = 0.066$, $k_0 = 6h^{-1}$ (Yellow line), k_1= $1.3h^{-1}$ (Blue line), $2h^{-1}$ (Green line), $2.6h^{-1}$ (Red line) or $3.34h^{-1}$ (Cyan line), ϕ_m= 0.0061, $k_3 = 0.3h^{-1}$, $C = 5 \times 10^5$ Miller units.

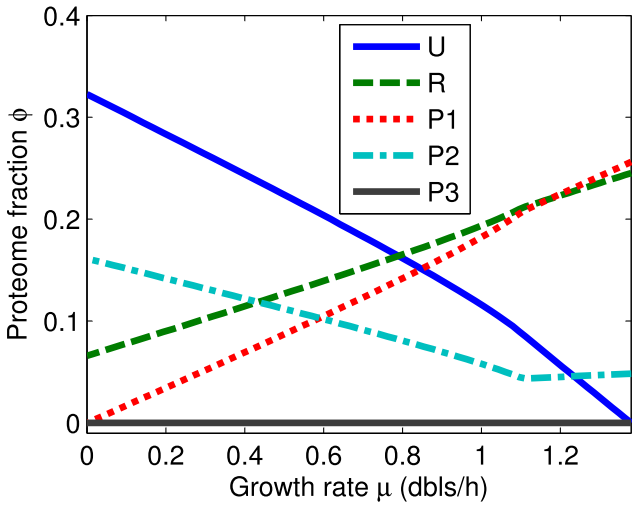

Figure S9: The model predicts the relation of the proteome fraction of each class proteins and growth rate under overexpression of unnecessary protein. Parameters: $\phi^* = 0.55$, $\phi_0 = 0.066$, $k_0 = 6$, $\phi_m = 0.0061$, $k_3 = 0.3h^{-1}$, $\alpha = 0.5$, k_1=4.2h^{-1}.

Supporting Tables

Table S1: Assumptions and parameters in the model for all the stresses studied here.

specific stress	major assumptions		parameters	
	common	specific	chosen based on literature (3)	fixed by fitting data †
AA supply stress	J_2 and J_4 are proportional to the concentration of unfolded polypeptides (ψ_{UP}) and Michaelis-Menten functions of the concentration of chaperones (ψ_{P2}).	k_1 is decreased.	ϕ^*, ϕ_0, k_0	ϕ_m, k_3, C
translation inhibition		k_0 is decreased.	ϕ^*, ϕ_0, k_1	ϕ_m, k_3, C
acidic/oxidative stress		k_1 and $1/\phi_m$ are decreased as Hill functions of stress intensity.	ϕ^*, ϕ_0, k_0, k_1^*	ϕ_m^*, k_3, K_x, β, C
overexpression of unnecessary protein		The mass fraction of unoptimized chaperones is proportional to that of expressed unnecessary protein	ϕ^*, ϕ_0, k_0, k_1	ϕ_m, k_3, α.

† Notice that the same parameters, i.e. ϕ_m (ϕ_m^*), k_3 and C, under different stresses were assigned the same values in the fitting.

Table S2: Experimental data and error estimates for Fig. 5 *A*.

Medium[a]	Growth rate (dbls/h)[b]	β-gal activity (10^5 Miller units)
M9+Glyc	0.54±0.02	2.03±0.07
+0.25μL/mL GAA[c]	0.57±0.01	2.02±0.06
+0.50μL/mL GAA	0.51±0.01	2.00±0.03
+0.75μL/mL GAA	0.41±0.01	2.02±0.07
+1.00μL/mL GAA	0.31±0.01	2.19±0.01
M9+Gluc	0.81±0.02	1.56±0.20
+0.25μL/mL GAA	0.81±0.03	1.42±0.20
+0.50μL/mL GAA	0.76±0.02	1.51±0.30
+0.75μL/mL GAA	0.62±0.01	1.51±0.40
+1.00μL/mL GAA	0.51±0.03	1.78±0.06
+1.25μL/mL GAA	0.33±0.03	2.01±0.20
M9+cAA+Glyc	0.86±0.02	1.32±0.01
+0.25μL/mL GAA	0.80±0.02	1.30±0.04
+0.50μL/mL GAA	0.69±0.01	1.31±0.04
+0.75μL/mL GAA	0.60±0.01	1.34±0.05
+1.00μL/mL GAA	0.50±0.01	1.38±0.05
+1.25μL/mL GAA	0.40±0.01	1.48±0.10
M9+cAA+Gluc	1.15±0.01	1.36±0.05
+0.25μL/mL GAA	1.08±0.02	1.30±0.05
+0.50μL/mL GAA	0.98±0.02	1.30±0.10
+0.75μL/mL GAA	0.80±0.02	1.21±0.06
+1.00μL/mL GAA	0.70±0.03	1.17±0.01
+1.25μL/mL GAA	0.50±0.03	1.24±0.04

a.Abbreviations: **M9+Glyc** - M9+0.5% (v/v) glycerol; **M9+Gluc** - M9+0.5% (w/v) glucose; **M9+cAA+Glyc** - M9+0.2% (w/v) casamino acids+0.5% (v/v) glycerol; **M9+cAA+Gluc** - M9+0.2% (w/v) casamino acids+0.5% (w/v) glucose.
b. The value behind ± indicates standard deviation among three or more replicates in one measurement. (Repeated measurements done on different days show similar patterns in the relation of β-gal activity and growth rate).
c.**GAA**-Glacial acetic acid.

Table S3: Experimental data and error estimates for Fig. 5 *B*.

Medium[a]	Growth rate (dbls/h)[b]	β-gal activity (10^5 Miller units)
M9+Glyc	0.55±0.01	1.82±0.05
+0.20μM Pd[c]	0.50±0.01	1.85±0.06
+0.25μM Pd	0.22±0.03	1.79±0.14
+0.30μM Pd	0.12±0.01	1.99±0.22
M9+Gluc	0.79±0.02	1.60±0.04
+0.20μM Pd	0.65±0.02	1.71±0.13
+0.25μM Pd	0.56±0.03	1.64±0.10
+0.30μM Pd	0.40±0.09	1.60±0.11
M9+cAA+Glyc	0.89±0.03	1.68±0.14
+1 μM Pd[d]	0.79±0.02	1.76±0.11
+5 μM Pd	0.65±0.01	1.73±0.13
+20μM Pd	0.54±0.01	1.85±0.09
+30μM Pd	0.42±0.02	2.21±0.18
+35μM Pd	0.35±0.01	2.25±0.19
M9+cAA+Gluc	1.19±0.04	1.46±0.06
+1 μM Pd	0.90±0.03	1.19±0.05
+5 μM Pd	0.82±0.01	1.18±0.05
+20μM Pd	0.78±0.02	1.18±0.08
+40μM Pd	0.66±0.03	1.34±0.03

a.Abbreviations: **M9+Glyc** - M9+0.5% (v/v) glycerol; **M9+Gluc** - M9+0.5% (w/v) glucose; **M9+cAA+Glyc** - M9+0.2% (w/v) casamino acids+0.5% (v/v) glycerol; **M9+cAA+Gluc** - M9+0.2% (w/v) casamino acids+0.5% (w/v) glucose.
b.The value behind ± indicates standard deviation among three or more replicates in one measurement. (Repeated measurements done on different days show similar patterns in the relation of β-gal activity and growth rate.)
c.**Pd** - Paraquat dichloride.

Table S4: Experimental data and error estimates for Fig. S8 *A*.

Medium[a]	Growth rate (dbls/h)[b]	β-gal activity (10^5 Miller units)
M9+Glyc	0.54±0.01	1.84±0.10
+1μM Cm[c]	0.58±0.01	1.57±0.05
+2μM Cm	0.56±0.01	1.35±0.05
+4μM Cm	0.43±0.01	1.16±0.06
+6μM Cm	0.37±0.01	0.98±0.06
+8μM Cm	0.31±0.01	0.86±0.05
M9+Gluc	0.83±0.02	1.48±0.04
+1μM Cm	0.82±0.02	1.48±0.08
+2μM Cm	0.75±0.01	1.44±0.11
+4μM Cm	0.63±0.01	1.15±0.07
+6μM Cm	0.52±0.01	1.13±0.05
+8μM Cm	0.45±0.01	0.98±0.07
M9+cAA+Glyc	0.88±0.03	1.49±0.04
+1μM Cm	0.87±0.02	1.24±0.03
+2μM Cm	0.76±0.01	1.06±0.04
+4μM Cm	0.54±0.02	0.84±0.09
+6μM Cm	0.43±0.02	0.64±0.03
+8μM Cm	0.34±0.01	0.69±0.04
M9+cAA+Gluc	1.21±0.03	1.36±0.06
+1μM Cm	1.15±0.03	1.23±0.05
+2μM Cm	1.00±0.01	1.08±0.02
+4μM Cm	0.74±0.02	1.00±0.05
+6μM Cm	0.60±0.01	0.72±0.03
+8μM Cm	0.48±0.01	0.66±0.03

a.Abbreviations: **M9+Glyc** - M9+0.5% (v/v) glycerol; **M9+Gluc** - M9+0.5% (w/v) glucose; **M9+cAA+Glyc** - M9+0.2% (w/v) casamino acids+0.5% (v/v) glycerol; **M9+cAA+Gluc** - M9+0.2% (w/v) casamino acids+0.5% (w/v) glucose.

b. The value behind $\pm$ indicates standard deviation among three or more replicates in one measurement. (Repeated measurements with not exactly same protocols show similar patterns in the relation of β-gal activity and growth rate.)

c.**Cm**-chloramphenicol.